Helical magnetic state in the distorted triangular lattice of α-$CaCr_2O_4$

L. C. Chapon,[1] P. Manuel,[1] F. Damay,[2] P. Toledano,[3] V. Hardy,[4] and C. Martin[4]

[1]*ISIS facility, STFC Rutherford Appleton Laboratory, Chilton, Didcot, Oxfordshire, OX11-0QX,United Kingdom*

[2]*Laboratoire Leon Brillouin, CEA-CNRS, UMR 12, CEA-Saclay, F-91191 Gif-sur-Yvette Cedex, France*

[3]*Laboratory of Physics of Complex Systems, University of Picardie, 33 rue Saint-Leu, F-80000 Amiens, France*

[4]*Laboratoire CRISMAT, ENSICAEN, UMR F-6508 CNRS, 6 Boulevard du Marechal Juin, F-14050 Caen Cedex, France*

(Received 29 June 2010; published 24 January 2011)

The magnetic properties of the high temperature α form of the $CaCr_2O_4$ compound have been investigated for the first time by magnetic susceptibility, specific heat, and powder neutron diffraction. The system undergoes a unique magnetic phase transition at 43 K to a long-range ordered incommensurate helical phase with magnetic propagation vector $\mathbf{k} = (0,0.3317(2),0)$. The magnetic model proposed from neutron diffraction data shows that the plane of rotation of the spins is perpendicular to the wave vector and that the magnetic modulation is consistent with two modes belonging to distinct irreducible representations of the group. The magnetic point group $2221'$ is not compatible with ferroelectricity unlike the $CuCrO_2$ delafossite [Kimura *et al.*, Phys. Rev. B, **78** 140401 (2008)], but predicts the existence of quadratic magnetoelectric effects, discussed based on a Landau analysis.

DOI: 10.1103/PhysRevB.83.024409 PACS number(s): 71.30.+h, 75.47.Lx, 75.10.−b

I. INTRODUCTION

In recent years, spin-driven ferroelectricity and giant magnetoelectric effect have been found in a variety of frustrated magnets, in particular in systems that develop long-wavelength magnetic modulations such as cycloidal or helicoidal states, incommensurate or not with the crystalline lattice. Most of the attention was initially focused on cycloidal magnets such as $TbMnO_3$ (Ref. 1) for which the inverse Dzyaloshinskii-Moriya[2] and spin-current models[3] predict the onset of a spontaneous polarization when the direction of the modulation (**k** vector) is perpendicular to the spin-rotation axis (**e**).[4] More recent work on incommensurate magnetic phases in triangular lattices[5–10] has established that improper ferroelectric orders of similar magnitudes can also appear in spin spiral magnets, that is, systems that possess a true magnetic chirality (**k** parallel to **e**), however, requiring another microscopic coupling mechanism such as the hybridization effects proposed by Arima.[11] Those systems are quasi-two-dimensional triangular lattices and display a nearly 120° magnetic arrangement in the triangular layers as expected for Heisenberg spins. Improper ferroelectricity predicted by symmetry[10] arguments depends only on the orientation of **e** with respect to the crystal axes, often dictated by weak single-ion anisotropy terms.

In this paper, we report for the first time on the magnetic properties of α-$CaCr_2O_4$ whose orthorhombic crystal structure[12] is closely related to the structure of delafossites, with the exception of a small distortion of the triangular lattice. The magnetic susceptibility indicates strong antiferromagnetic correlations (Weiss temperature of −688.5 K) and a unique transition to a long-range ordered state at $T_N = 43$ K. The specific heat displays a sharp and intense peak around 43 K, consistent with a unique transition. Powder neutron diffraction proves the existence of long-range magnetic order below T_N, incommensurate with the crystal lattice with propagation vector $\mathbf{k} = (0,0.3317(2),0)$. The model proposed for the magnetic structure, derived from the neutron data and symmetry considerations, corresponds to a nearly 120° *out-of-plane* helix, with **e** perpendicular to **k**. Symmetry analysis using the complete irreducible corepresentations of the wave-vector group shows that the point group symmetry of the magnetic state is $2221'$ and can be only stabilized through two successive second-order transitions or through a first-order transition. While in the rhombohedral delafossite such an out-of-plane spiral leaves a polar point group, here the spin chirality preserves all proper rotations, predicting the absence of electric polarization at T_N. However, we show through a Landau analysis of the magnetoelectric free energy that quadratic magnetoelectric effects are allowed by symmetry and should be observed in low magnetic fields.

II. EXPERIMENT

The synthesis of polycrystalline α-$CaCr_2O_4$ followed a two-step process. A sample of β-$CaCr_2O_4$ was first prepared in the shape of a rod (6 millimeters in diameter and several centimeters in length), starting from a 1:1 mixture of CaO and Cr_2O_3 heated at 1400°C for 12 hours in an argon flow. This rod was heated in an argon atmosphere by using an image furnace to obtain the high temperature conditions ($T > 1700$°C), but without reaching the melting temperature. Magnetic susceptibility has been measured using a Superconducting Quantum Interference Device (SQUID, Quantum Design®) in a magnetic field of 100 Oe on warming following a zero-field cooling process. Heat capacity measurements [C(T)] were carried out in a Physical Property Measurement System (PPMS, Quantum Design®) using a semi-adiabatic relaxation method.[13] Two types of procedures were followed to record zero-field C(T) curves: (i) Equally spaced data points registered upon warming and using a small temperature rise of the order of 0.4 K around the transition. The analysis is the standard one in which the so-called 2τ model[14] is used to fit at once both the heating and cooling branches at each point; (ii) a large single-pulse method described in Ref. 15 where the temperature is swept across the complete width of the transition, either warming or cooling (temperature rise of 5 K). It this case, the heat capacity is derived from a point-by-point analysis of the time response along each of the two branches. In case of a first-order transition, it is known that

the former method can yield spurious results,[16,17] whereas the latter is able to account for both the latent heat and hysteretical features.[15] Neutron diffraction experiments were collected on the WISH diffractometer of the ISIS Facility, Rutherford Appleton Laboratory (UK). Data have been focused on five histograms from detector banks covering 32° each, and are shown for the bank centered at $2\theta = 90°$. A 0.55 g sample was placed in a thin wall (30 μm) vanadium cylindrical can mounted in a helium cryostat. Diffractograms have been recorded in the paramagnetic regime at 70, 1.5 K, and warming in varying temperature steps. Rietveld refinements of the neutron data have been performed with the FULLPROF program.[18]

III. RESULTS

The crystal structure of α-$CaCr_2O_4$ was first reported by Pausch *et al.*.[12] It crystallizes with orthorhombic symmetry, confirmed by our electron microscopy measurements (not shown) in the space group *Pmmn* (Fig. 1). The structure refined from our neutron diffraction data in the paramagnetic regime at 70 K is also consistent with the earlier work.[12] There are two inequivalent Cr sites, Cr_1 located at (0,0,0), of $\bar{1}$ symmetry and Cr_2 at position [0.5047(6), $\frac{1}{4}$, 0.497(1)] located on a mirror plane, each site of multiplicity four. The Cr ions are six-coordinated by oxygen in a distorted octahedral configuration. The octahedra share edges to form CrO_2 layers in the *bc* plane, leaving a weakly distorted triangular lattice as shown by the different interatomic distances marked in Fig. 1. The CrO_2 layers, separated by Ca^{2+} ions, are stacked along the *a* axis of the orthorhombic unit cell. The in-plane magnetic interactions between Cr can be mediated either by direct exchange through the t_{2g} orbitals or by Cr-O-Cr superexchange interactions. The interactions between layers can be mediated by super-superexchange interactions through

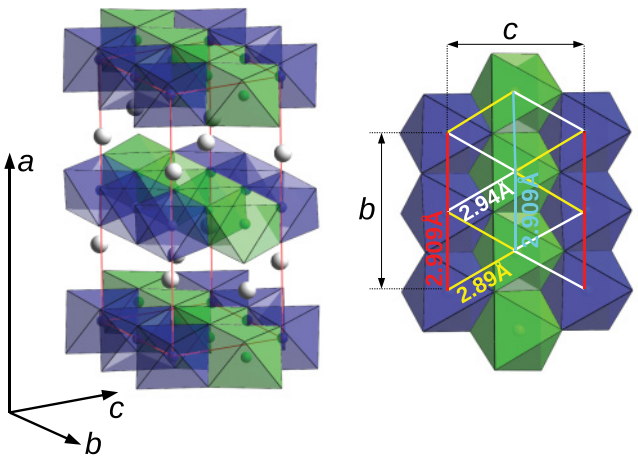

FIG. 1. (Color online) (Left) Crystal structure of α-$CaCr_2O_4$. CrO_6 octahedra are shown in blue and green colors for the inequivalent Cr_1 and Cr_2 sites (see text for details). The Ca^{2+} ions are shown as light gray spheres. The red thin line marks the crystallographic unit cell. (Right) Projection of the CrO_2 layer onto the *bc* plane. Colored thick lines shows the connectivity between first-neighbor Cr ions. The corresponding interactomic distances are shown.

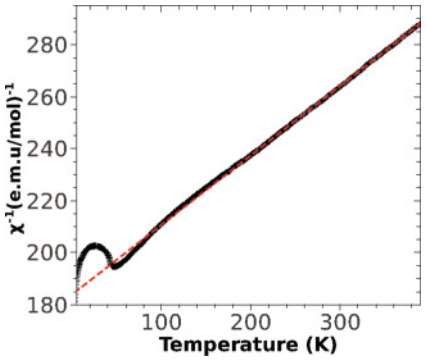

FIG. 2. (Color online) Inverse molar magnetic susceptibility of α-$CaCr_2O_4$ as a function of temperature under a magnetic field of 100 Oe. The line is a linear fit with a Curie-Weiss law.

two oxygen atoms, but are expected to be much weaker due to the large interatomic Fe-Fe distance (5.52 Åat 1.5 K).

The inverse magnetic susceptibility (Fig. 2) shows a quasilinear regime above 200 K. A linear fit of the data with a Curie-Weiss law in the temperature range 200 to 390 K yields a paramagnetic moment of $3.869(1)\mu_B$ per Cr^{3+} ion, and a Weiss temperature of $-688.5(5)$ K. The value of the paramagnetic moment is in perfect agreement with the expected value of $3.87\mu_B$ for a pure spin contribution ($S = 3/2$) of Cr^{3+}. The strongly negative Weiss temperature indicates large antiferromagnetic (AFM) interactions. On cooling below 200 K, one observes a deviation of the inverse susceptibility from the nearly linear regime followed at $T_N = 43$ K by a more abrupt drop indicative of long-range AFM ordering. There is no evidence of additional transitions from susceptibility measurements at different fields (not shown). The large difference between the value of the Weiss temperature and T_N is inherent to the reduction of dimensionality in this pseudo-two-dimensional system as well as magnetic frustration imposed by the triangular geometry.

The left panel of Fig. 3 displays the specific heat, C(T), recorded from the standard and single-pulse methods (see experimental section), while the inset is an enlargement exhibiting the shift between the warming and cooling branches derived from the latter technique. At $T_N = 43$ K, a very sharp peak is observed with a full width at half maximum of about 0.5 K. Using a Debye function to fit the high temperature data as an approximation of the lattice specific heat, one can derive the temperature dependence of the magnetic entropy (S_m) shown in the right panel of Fig. 3. There is a clear kink at T_N on the Sm(T) curve, but judging the nature of the transition from this feature only is difficult. The Sm(T) around the transition (Fig. 3, inset) can indeed be regarded either as a broadened jump expected for a first-order transition (FOT) in real materials (i.e., nonideals with the presence of defects) or as a knee typical of a second-order transition (SOT). Two other experimental observations must be considered: First, the nearly perfect superimposition of the C(T) curves derived from the single-pulse and standard method, while a substantial part of the latent heat—if present—is supposed to be invisible in the latter technique.[15] Second, the temperature shift observed between the heating and cooling data in the single-pulse method is very small and cannot even be safely ascribed to

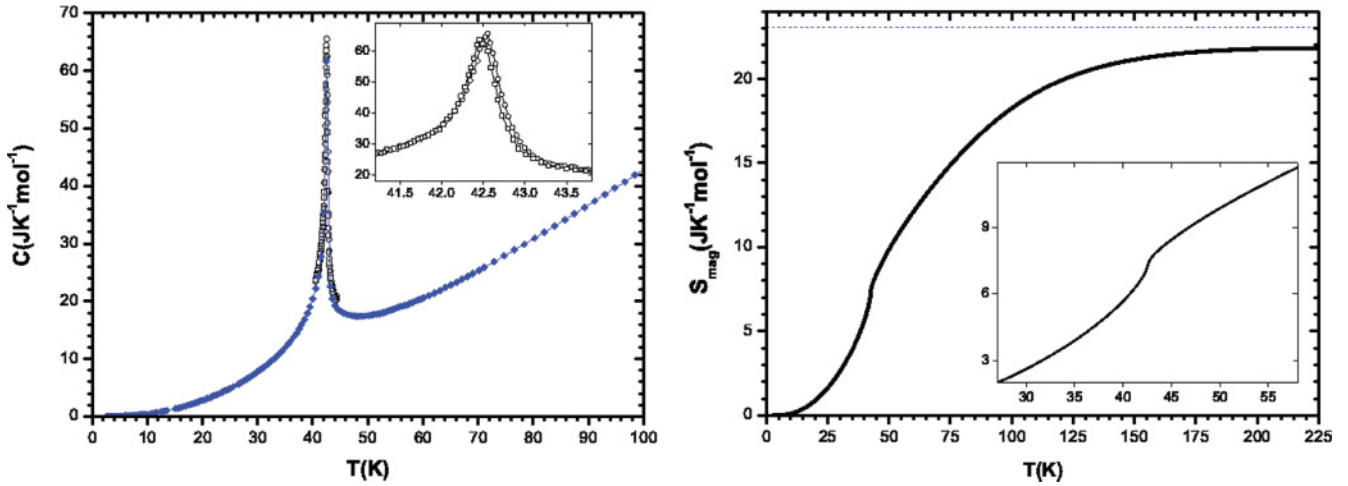

FIG. 3. (Color online) (Left) Specific heat of α-$CaCr_2O_4$ in zero magnetic field measured by the standard (filled diamonds), single pulse method (open circles), and SPM cooling (open squares) (see text for details of the various techniques). (Right) Magnetic entropy obtained by subtracting the lattice contribution estimated by a Debye function to the total specific heat. The inset focus on the temperature region close to T_N. The dashed line indicates the theoretical limit of $2R\ln(4)$.

a genuine hysteresis as encountered in most of the FOT's. In fact, it appears that this hysteresis quantitatively corresponds to the expected temperature lag between the sample and the platform which contains the thermometer. At this stage, one must conclude that the transition at T_N is either a SOT or a very weak FOT.

Below 43 K, long-range magnetic order is detected by the presence of five additional Bragg peaks in the powder neutron diffraction data, the most intense close to a d spacing of 4.5 Å. The intensity of these peaks decreases with the modulus of the scattering vector (Q) in agreement with the expected Q dependence of the magnetic form factor. To determine the periodicity of the magnetic structure, an automatic indexing procedure using a grid search[18] was employed but failed to give a satisfactory solution due to the presence of pseudotrigonal symmetry. However, the magnetic peaks could all be indexed by exploring the reciprocal space in the vicinity of the special k vector expected for a 120° structure in an isotropic triangular lattice, corresponding to $\mathbf{k} = (0, \frac{1}{3}, 0)$ in the α-$CaCr_2O_4$ orthorhombic unit cell. Further analysis shows that the magnetic structure is actually incommensurate with a propagation vector $\mathbf{k} = (0, 0.3317(2), 0)$, labeled k_8 in Kovalev's notation.[19] The incommensurability, albeit small, is genuine as indicated by the inferior refinement presented in Fig. 4 showing an offset for the position of the magnetic peak (most noticeable in the difference curve) when the value is locked at $\mathbf{k} = (0, \frac{1}{3}, 0)$. The magnetic peaks have an almost purely Lorentzian profile, with widths much larger than the instrumental resolution, indicating short correlations lengths. To account for the observed profile and derive an accurate value for the moment magnitudes, the Rietveld refinement of the magnetic phase was conducted using a phenomenological description of the peak broadening by a spherical harmonics expansion consistent with the Laue class mmm.

Symmetry analysis using the group of the propagation vector (little group) shows that the magnetic representation for each Cr sites is decomposed in four irreducible representations, labeled τ_1 to τ_4 according to Kovalev's tables.[19] The magnetic structure is only compatible with a model that mixes a basis vector along the (1,0,0) direction that transforms as τ_1, and a basis vector along (0,0,1) that transforms as τ_2. In this orthorhombic symmetry, the intensity of the diffraction pattern

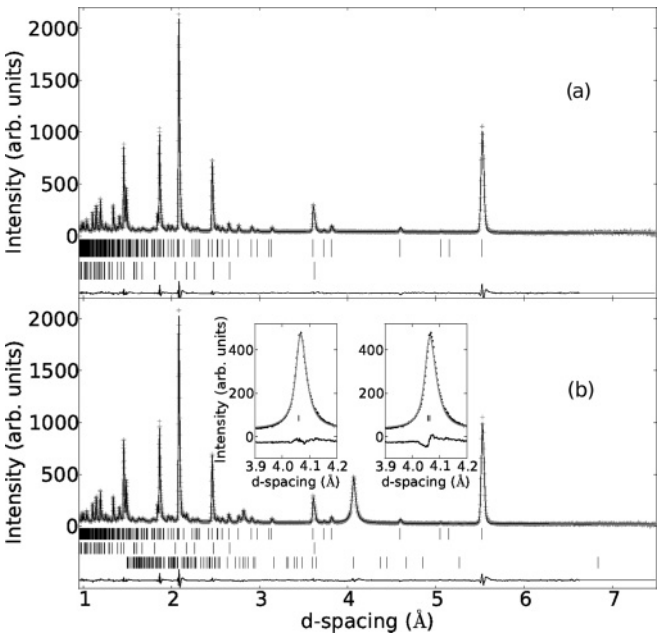

FIG. 4. Rietveld refinements of the neutron diffraction data collected in the paramagnetic phase at (a) 70 K and in the magnetically ordered phase at (b) 1.5 K. The data are shown as gray points and the result of the refinements as continuous black lines. The curves shifted below represent the differences between the observed and calculated patterns. In both panels, the top two rows of tick marks indicate the positions of Bragg peaks for the phases α-$CaCr_2O_4$ and the impurity Cr_2O_3. In panel (b), the third row of tick marks indicates the positions of magnetic Bragg peaks with propagation vector $k = (0, 0.3317(2), 0)$. The inset shows an enlarged region around the most intense magnetic peaks fitted using the incommensurate k vector (left) and commensurate one (right) $k = (0, \frac{1}{3}, 0)$.

is not sensitive to the relative phase between these two modes, that is, one cannot directly discriminate between a transversally polarized spin-density wave with the moments pointing in the *ac* plane (mixing the two basis vectors with coefficients of the same characters) or a helical modulation with the moment rotating in the *ac* plane (mixing the two basis vectors with coefficients of different characters, real and imaginary). However, at 1.5 K the refined amplitudes of the magnetic modes along the *a* and *c* axes were found to be 2.31(1) μ_B. If these modes were in phase (spin-density wave) the amplitude of the modulation will largely exceed the fully ordered moment of 3 μ_B expected for a pure spin-state Cr^{3+} ion. On this ground, it appears that the helical modulation is the only possible model to account for the observed pattern. It is also physically sensible as the entropy of a helical structure with constant moments is more favorable at low temperature than an amplitude modulated structure. The magnitudes of the magnetic moments were found to be similar for the two symmetry inequivalent Cr sites, and final refinements were conducted imposing such constraint, even if the latter is not directly imposed by symmetry. Finally, the relative phase between the modulation for sites 1 and 2 is a free parameter, as these sites are not related by symmetry operations of the group. The phase has been refined to a value very close to $-\frac{\pi}{3}$ and was constrained to this specific value in the final refinement. The magnetic structure, shown in Fig. 5, is made of nearly 120° configuration in each triangle, propagating as spirals along the *b* axis of the unit cell with the two spirals per unit cell (on different Cr sites) of the same chirality. Unlike cycloidal modulations, this proper spiral structure possesses a true handedness. The coupling between adjacent CrO_2 layers, mediated through super-superexchange interactions, is antiferromagnetic. The magnetic structure is similar to that found in delafossites[6,10] (i.e., the 120° configuration is *out-of-plane*). However, symmetry considerations lead to different coupling between magnetic order parameters and electric order than the delafossite, which will be discussed later. The ordered magnetic moment varies smoothly with temperature (Fig. 5), but the critical exponent was found to be ∼1/4, deviating largely from the mean-field limit and reminiscent to that found in first-order phase transitions.[20] Within the temperature resolution of our experiment there is a unique transition at T_N, in agreement with measurements of the magnetic susceptibility and specific heat.

The magnetic model consists of a mixing of two modes belonging to two different irreducible representations (i.e., the transition from the paramagnetic phase to the incommensurate magnetic phase can be fully described by considering

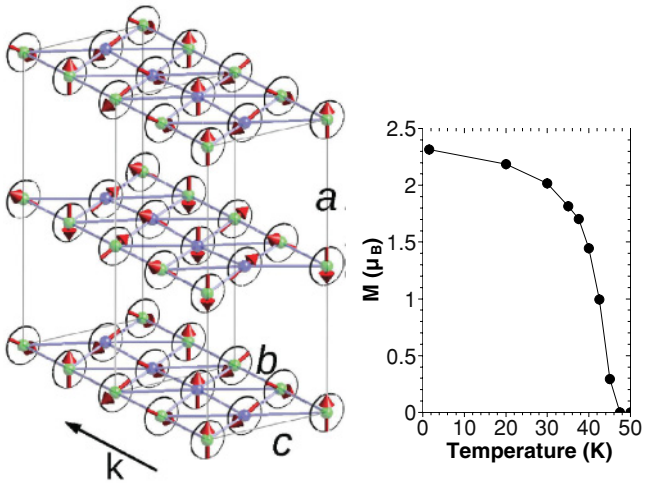

FIG. 5. (Color online) (Left) Magnetic structure of α-$CaCr_2O_4$. The two independent Cr sites are shown with different colors (light green for Cr_1 and light blue for Cr_2). Two unit cells along the *b* axis, marked by thin black lines, are shown. The axes are labeled in italic and the direction of the magnetic propagation vector (k) is shown by the arrow. (Right) Temperature dependence of the ordered magnetic moment on the Cr ions.

two two-dimensional complex order parameters $\eta_1 = \rho_1 e^{i\phi_1}$, $\eta_1^* = \rho_1 e^{-i\phi_1}$ and $\eta_2 = \rho_2 e^{i\phi_2}$, $\eta_2^* = \rho_2 e^{-i\phi_2}$). The matrix representatives of the complete irreducible corepresentations of the group of **k** are presented in Table I. The time-reversal operator 1′, the matrix of which is not shown, needs also to be considered to be able to write the Landau energy. Considering these two magnetic order parameters, the expansion of the Landau free energy F is written

$$F = F_0 + \frac{1}{2}\alpha_1\rho_1^2 + \frac{1}{2}\alpha_2\rho_2^2 + \frac{1}{4}\beta_1\rho_1^4 + \frac{1}{4}\beta_2\rho_2^4 + \gamma\rho_1^2\rho_2^2\cos(2\phi) + \cdots, \quad (1)$$

where the α_i, β_i ($i = 1,2$) and γ are coefficients of the Taylor expansion and $\phi = \phi_1 - \phi_2$ is the phase difference between the two modes. Minimization of F with respect to ρ_1 and ρ_2 leads to five distinct magnetic states that can be stabilized from the paramagnetic space group $Pmmn1'$. The point groups of these five magnetic states are shown in Fig. 6 together with their stability conditions. The structure observed experimentally corresponds to both order parameters being nonzero and $\phi = \pi/2$ (mixing of two modes in phase quadrature) and has the point symmetry 2221′. The 1′ operator is contained in the point group of any incommensurate structure since its

TABLE I. Matrix representatives of the complete irreducible corepresentations Δ_1 and Δ_2 associated with the irreducible representations of the little group τ_1 and τ_2[19] (see text for details). The matrices act each on the two-dimensional spaces spanned by the complex order parameters, respectively, (η_1,η_1^*) and (η_2,η_2^*). The matrix for time reversal is not shown.

Irrep.	$\{2_x\|\frac{1}{2}\,00\}$	$\{2_y\|0\frac{1}{2}0\}$	$\{2_z\|\frac{1}{2}\frac{1}{2}0\}$	$\{\bar{1}\|000\}$	$\{m_y\|\frac{1}{2}\,00\}$	$\{m_{xz}\|0\frac{1}{2}\,0\}$	$\{m_{xy}\|\frac{1}{2}\frac{1}{2}\,0\}$	$\{1\|010\}$
Δ_1	$\begin{pmatrix}0 & 1\\ 1 & 0\end{pmatrix}$	$\begin{pmatrix}\epsilon & 0\\ 0 & \epsilon^*\end{pmatrix}$	$\begin{pmatrix}0 & \epsilon^*\\ \epsilon & 0\end{pmatrix}$	$\begin{pmatrix}0 & 1\\ 1 & 0\end{pmatrix}$	$\begin{pmatrix}1 & 0\\ 0 & 1\end{pmatrix}$	$\begin{pmatrix}0 & \epsilon^*\\ \epsilon & 0\end{pmatrix}$	$\begin{pmatrix}\epsilon & 0\\ 0 & \epsilon^*\end{pmatrix}$	$\begin{pmatrix}\epsilon^2 & 0\\ 0 & \epsilon^{*2}\end{pmatrix}$
Δ_2	$\begin{pmatrix}0 & -1\\ -1 & 0\end{pmatrix}$	$\begin{pmatrix}\epsilon & 0\\ 0 & \epsilon^*\end{pmatrix}$	$\begin{pmatrix}0 & -\epsilon^*\\ -\epsilon & 0\end{pmatrix}$	$\begin{pmatrix}0 & 1\\ 1 & 0\end{pmatrix}$	$\begin{pmatrix}-1 & 0\\ 0 & -1\end{pmatrix}$	$\begin{pmatrix}0 & \epsilon^*\\ \epsilon & 0\end{pmatrix}$	$\begin{pmatrix}-\epsilon & 0\\ 0 & -\epsilon^*\end{pmatrix}$	$\begin{pmatrix}\epsilon^2 & 0\\ 0 & \epsilon^{*2}\end{pmatrix}$

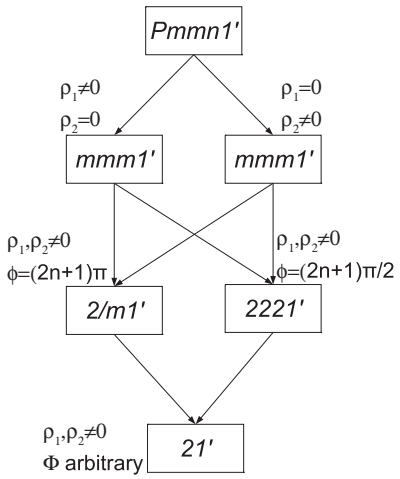

FIG. 6. Phase diagram of the possible magnetic point groups that can be stabilized from the paramagnetic group $Pmmn1'$ by considering two order parameters η_1 and η_2 transforming, respectively, as the τ_1 and τ_2 representations (see text for details).

application (phase of π) is always equivalent to a translation. The phase $2221'$ can be stabilized from the paramagnetic state either through two successive second-order phase transitions as indicated by the arrow in Fig. 6 or through a single first-order phase transition. According to our data showing a unique critical point but no pronounced hysteresis, we assumed that the transition must be *weakly* first order. One should note that the only possibility to stabilize the observed magnetic phase through a SOT would be to consider a symmetry for the exchange Hamiltonian that is higher than the crystal symmetry (for example, considering a Heisenberg Hamiltonian). In such a case, the symmetry analysis shows that the two irreducible representations involved, τ_1 and τ_2, belong to the same exchange multiplet. However, this is rarely observed and always a case of pseudosymmetry. In the following discussion we will assume that the crystal symmetry is the relevant basis of work and that the transition is weakly first-order.

The Landau theory of transitions with two order parameters that are coupled biquadratically has been studied by several authors[21,22] and reviewed by Toledano *et al.*.[23] The invariant as written in Eq. (2) is not sufficient to stabilize a FOT $Pmmn1' \rightarrow 2221'$, which would have to occur at a single point in the parameter space. To stabilize this transition through a line in phase space, one needs to consider a strongly negative coupling term γ and at least one positive six degree term (for example, $\delta\rho_1^6$). In such conditions, considering that the first coefficient α_1 follows the usual temperature dependence $\alpha_1 = \alpha(T - T_c)$ with $\alpha > 0$, and that ρ_1 is the driving order parameter, the critical behavior of ρ_2 follows the triggering mechanism first discussed by Holakovsky.[21] Calculations show that it is equivalent to consider the canonical free energy

$$F = F_0 + \tfrac{1}{2}\alpha_1\rho_1^2 + \tfrac{1}{4}\beta_1\rho_1^4 + \tfrac{1}{6}\gamma_1\rho_1^6, \qquad (2)$$

with $\alpha_1 = \alpha(T - T_c)$ with $\alpha > 0$, $\beta_1 < 0$, and $\gamma_1 > 0$. In fact, the triggering parameter ρ_2 has for its only effect to add mutiplicative and additive constants in the numerical expressions found for all thermodynamic variables using Eq. (2). The stability condition of Eq. (2) yields the temperature dependence of ρ

$$\rho_1(T) \approx M(T) = \left(\frac{-\beta_1 + \sqrt{\beta_1^2 - 4\alpha_1\gamma_1}}{2\gamma_1}\right)^{\frac{1}{2}-\delta}, \qquad (3)$$

where $0 < \delta < \frac{1}{4}$ is an *ad hoc* parameter that accounts for the deviation from the tricritical point ($\delta = \frac{1}{4}$). The specific heat below T_N is then

$$C_p(T) = -T\frac{\partial^2 F(T)}{\partial T^2} = C_p^0(T) + \frac{\alpha^2 T}{[\beta_1^2 - 4\alpha\gamma_1(T - T_N)]^{\frac{1}{2}-\delta}}, \qquad (4)$$

where $C_p^0(T)$ is the specific heat above T_N. The experimental specific heat has been successfully fitted with Eq. (4) (Fig. 7) in the temperature range 33.5–42.5 K. We found the three independent parameters $\beta_1^2 = 0.32(2)$, $\alpha\gamma_1 = 0.59(3)$, and $\delta = 0.11(1)$. It is important to note that the quickly decaying specific heat below T_N related to the exponent $(0.5\text{-}\delta)$ is not compatible with a SOT (for which a linear variation is expected). From the fitted parameters, one can estimate the width of the hysteresis given by the expression $\Delta T = \frac{\beta_1^2}{4\alpha\gamma_1} = 0.13$ K. This very small hysteresis is compatible with the results of specific heat showing that ΔT is extremely small.

The symmetry of this helical phase in such orthorhombic symmetry is extremely interesting. As already mentioned, the point group $2221'$, although not centrosymmetric, is not polar and therefore forbids a spontaneous polarization at the magnetic transition. Since the structure is incommensurate and the time-reversal operator is present in the point group, the linear magnetoelectric effect is also forbidden. However, invariants that are linear in the electric field (E) and quadratic in the magnetic field (H) are allowed by symmetry (while terms in HHE are forbidden). The quadratic magnetoelectric effect is described by a third-rank tensor, β_{ijk} symmetric in the last two indices, and where i is the direction of the electric field

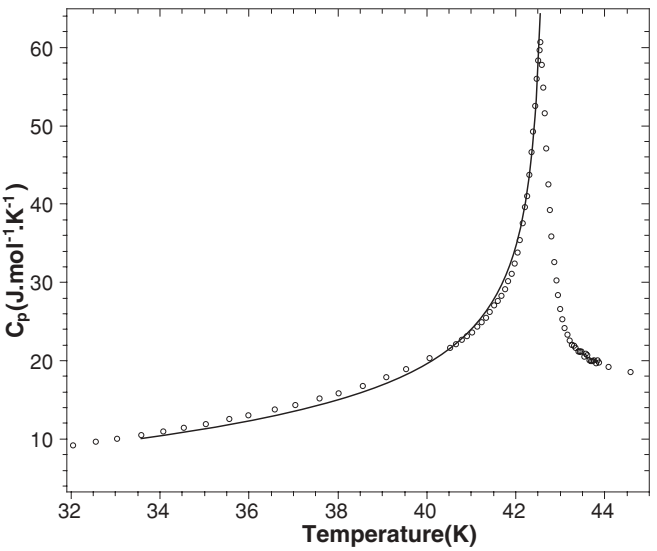

FIG. 7. Specific heat of α-$CaCr_2O_4$ in the low temperature region. The points are experimental data and the solid line represents the result of the refinement with Eq. (4).

and j and k indicate the direction of the magnetic fields. For the point group $2221'$ there are three terms allowed for this tensor that transform as the piezoelectric tensor, β_{123} ,β_{213}, and β_{312}. One can easily show using the matrix representatives of Δ_2 and Δ_3 given in Table I that the following mixed invariants of the magnetic order parameters with E and H can be constructed

$$F_{ME} = \rho_1\rho_2 \sin(\phi) \times [\beta_{123}E_xH_yH_z + \beta_{213}E_yH_xH_z + \beta_{312}E_zH_xH_y]. \quad (5)$$

This suggests that the application of low magnetic fields (if the system remains in the phase described by the symmetry of the zero-field phase) inclined with respect to the crystallographic axes will induce an electrical polarization whose magnitude will be proportional to the square of the magnetic field. Of course, the application of sufficiently large magnetic fields could drive the system to other symmetry phases. Single crystal specimens are necessary to determine the behavior of the electric properties and magnetic properties under a magnetic field.

It is important to realize that this result can be easily generalized to all incommensurate magnetic systems that possess a true magnetic handedness (i.e., all spirals in the unit cell propagate with the same chirality). In such systems and irrespective of the paramagnetic symmetry, all improper symmetry operations are lost in the magnetically ordered state and the time-reversal operator is preserved by the incommensurability, implying that at least one of the β_{ijk} is allowed and quadratic magnetoelectric effects are present. This magnetoelectric effect, even though of a higher degree in the expansion of the free energy than the well-studied linear effect, is not bounded by thermodynamic conditions (see Ref. 24 and references therein) and therefore interesting to investigate in prototype spiral magnets of the type discussed here.

In conclusion, measurements of the magnetic properties of α-$CaCr_2O_4$ and neutron powder diffraction have shown that this system is analog to the delafossite. Strong antiferromagnetic interactions in the triangular CrO_2 planes lead to long-range magnetic ordering below $T_N = 43$ K, with an incommensurate propagation vector $k = (0,0.3317(2),0)$. The model for the magnetic structure, based on refinement of the neutron diffraction data and symmetry considerations, is consistent with a helicoidal modulation and a nearly 120° configuration in each triangular plaquette. The mirror plane symmetries are broken by the helicoidal arrangement, leaving the point group $2221'$, which allows for quadratic magnetoelectric effects in all directions.

[1] M. Kenzelmann, A. Harris, S. Jonas, C. Broholm, J. Schefer, S. Kim, C. Zhang, S. Cheong, O. Vajk, and J. Lynn, Phys. Rev. Lett. **95** 087206 (2005).

[2] I. A. Sergienko and E. Dagotto, Phys. Rev. B **73**, 094434 (2006).

[3] H. Katsura, N. Nagaosa, and A. V. Balatsky, Phys. Rev. Lett. **95**, 057205 (2005).

[4] M. Mostovoy, Phys. Rev. Lett. **96**, 067601 (2006).

[5] M. Kenzelmann, G. Lawes, A. B. Harris, G. Gasparovic, C. Broholm, A. P. Ramirez, G. A. Jorge, M. Jaime, S. Park, Q. Huang, A. Y. Shapiro, and L. A. Demianets, Phys. Rev. Lett. **98**, 267205 (2007).

[6] K. Kimura, H. Nakamura, K. Ohgushi, and T. Kimura, Phys. Rev. B **78**, 140401 (2008).

[7] T. Kimura, J. C. Lashley, and A. P. Ramirez, Phys. Rev. B **73**, 220401 (2006).

[8] T. Nakajima, S. Mitsuda, S. Kanetsuki, K. Tanaka, K. Fujii, N. Terada, M. Soda, M. Matsuura, and K. Hirota, Phys. Rev. B **77**, 052401 (2008).

[9] T. Nakajima, S. Mitsuda, K. Takahashi, M. Yamano, K. Masuda, H. Yamazaki, K. Prokes, K. Kiefer, S. Gerischer, N. Terada, H. Kitazawa, M. Matsuda, K. Kakurai, H. Kimura, Y. Noda, M. Soda, M. Matsuura, and K. Hirota, Phys. Rev. B **79**, 214423 (2009).

[10] M. Poienar, F. Damay, C. Martin, V. Hardy, A. Maignan, and G. André, Phys. Rev. B **79**, 014412 (2009).

[11] T. Arima, J. Phys. Soc. Jpn. **76**, 073702 (2007).

[12] H. Pausch and H. K. Mller-Buschbaum, Z. Anorg. Allg. Chem. **405**, 113 (1974).

[13] PPMS Heat Capacity Option Users Manual, Quantum Design (2009).

[14] J. Hwang, K. Lin, and C. Tien, Rev. Sci. Instrum. **68**, 94 (1997).

[15] V. Hardy, Y. Brard, and C. Martin, J. Phys. Condens. Matter **21**, 075403 (2009).

[16] J. Lashley, M. Hundley, A. Migliori, J. Sarrao, P. Pagliuso, T. W. Darling, M. Jaime, J. Cooley, W. Hults, L. Morales, D. Thoma, J. Smith, J. Boerio-Goates, F. Woodfield, G. Stewart, R. Fisher, and N. Phillips, Cryogenics **43**, 369 (2003).

[17] A. Szewczyk, M. Gutowska, B. Dabrowski, T. Plackowski, N. P. Danilova, and Y. P. Gaidukov, Phys. Rev. B **71**, 224432 (2005).

[18] J. Rodriguez-Carvajal, Physica B **192**, 55 (1993).

[19] O. Kovalev, *Representation of the Crystallographic Space Groups* (Gordon and Breach Science Publishers, New York, 1993).

[20] J. Toledano and P. Toledano, *The Landau Theory of Phase Transitions* (World Scientific, Singapore, 1987).

[21] J. Holakovsky, Phys. Status Solidi b **56**, 615 (1973).

[22] Y. Ishibashi, J. Phys. Soc. Jpn. **63**, 2082 (1994).

[23] P. Toledano and V. Dmitriev, *Reconstructive Phase Transitions: In Crystals and Quasicrystals* (World Scientific Publishing, Singapore, 1996).

[24] W. Eerenstein, N. D. Mathur, and J. F. Scott, Nature (London) **442**, 759 (2006).